Analysis of Synchronization between Two Modules of Pulse Neural Networks with Excitatory and Inhibitory Connections

Takashi Kanamaru

Department of Basic Engineering in Global Environment,
Faculty of Engineering, Kogakuin University,
2665-1 Nakano, Hachioji-city, Tokyo 192-0015, Japan

Abstract

To study the synchronized oscillations among distant neurons in the visual cortex, the synchronization between two modules of pulse neural networks was analyzed using the phase response function. It was found that the inter-module connections from excitatory to excitatory ensembles tend to stabilize the anti-phase synchronization, and that the inter-module connections from excitatory to inhibitory ensembles tend to stabilize the in-phase synchronization. It was also found that the inter-module synchronization was more noticeable when the inner-module synchronization was weak.

1 Introduction

The average behavior of neurons often shows synchronized oscillations in many areas of the brain, *e.g.*, in the visual cortex (Gray & Singer, 1989), the hippocampus (Buzsáki, Horváth, Urioste, Hetke, & Wise, 1992; Bragin, Jandó, Nádasdy, Hetke, Wise, & Buzsáki, 1995), the auditory neocortex (Traub, Bibbig, LeBeau, Cunningham, & Whittington, 2005), and the entorhinal cortex (Cunningham, Davies, Buhl, Kopell, & Whittington, 2003), and they have attracted considerable attention in past 20 years. Synchronized oscillations with gamma frequency (20∼70 Hz) among nearby neurons with overlapping receptive fields have been observed in the visual cortex. Moreover, when correlated visual stimulations were presented, synchronized oscillations were observed even among distant neurons that had non-overlapping receptive fields and that were separated by 7mm. Based on such observations, it was proposed that the correlations among neuronal activities might be related to the binding of visual information (for reviews, see Gray (1994)).

Several mechanisms likely contribute to the generation of such synchronized oscillations in the visual cortex. First, the lateral geniculate nucleus (LGN) often provides oscillating inputs to the visual cortex. However, the range of projections from the LGN cannot explain the cortical synchronization among distant neurons. Therefore, the synchronized oscillations in the visual cortex are thought to be generated by an intra-cortical mechanism, and not by oscillating inputs from the LGN (Gray & Singer, 1989). However, it is unknown whether the oscillations are caused by the properties of single neurons or by intra-cortical network interactions. As for the theory that the oscillations are caused by the properties of single neurons, it was reported that chattering cells in the visual cortex show periodic bursts of gamma frequency, which might be related to the generation of oscillatory responses (Gray & McCormick, 1996). On the other hand, many physiological evidences support the theory that the oscillations are generated by intra-cortical network interactions (Jagadeesh, Gray, & Ferster, 1992; Gray 1994). In the hippocampus, it was reported that the network that contains inhibitory neurons contributes to the generation of oscillations (Buzsáki, Horváth, Urioste, Hetke, & Wise, 1992; Whittington, Traub, & Jefferys, 1995; Fisahn, Pike, Buhl, & Paulsen, 1998).

Concerning the generation of synchronized oscillations in the neuronal network, we have been studying pulse neural networks that are composed of excitatory neurons and inhibitory neurons. In previous studies, the dynamics of a single module consisting of a network were analyzed using the Fokker-Planck equation, and various synchronized firings were found depending on the values of the parameters (Kanamaru & Sekine, 2004, 2005). Such synchronized firings might be related to the synchronized oscillations among nearby neurons. In the present study, in order to elucidate the mechanism of synchronized oscillations among distant neurons, we analyzed the synchronization between two modules of networks, in which each module was composed of excitatory neurons and inhibitory neurons. Ermentrout and Kopell (1998) analyzed a similar network of two modules, each of which contained an excitatory cell (E-cell)

and an inhibitory cell (I-cell). The E-cell and I-cell each represented populations of neurons, and their dynamics obeyed the equations for the spiking neuron model. Therefore, the neurons in each population were assumed to be perfectly synchronized. However, when the neurons in each module are not perfectly synchronized but are partially synchronized (van Vreeswijk, 1996), their analysis cannot hold because each neuron in a module receives many pulses from other neurons in that module and from neurons in the other module. In our model, perfect synchronization is not realized because of noise; therefore, probabilistic representations are required to describe the dynamics of each module. In section 2, the definition of a module of pulse neural network is given, and its dynamics are analyzed using the Fokker-Planck equation. Some examples of synchronized firings are presented. In section 3, a system with two modules of networks is introduced, and the inter-module synchronization is analyzed using the phase response function (Kuramoto, 1984; Ermentrout & Kopell, 1991; Ermentrout, 1996; Ermentrout, Pascal, & Gutkin, 2001; Nomura, Fukai, & Aoyagi, 2003). As a result, it was found that the inter-module connections from excitatory to excitatory ensembles tend to stabilize the anti-phase synchronization, and the inter-module connections from excitatory to inhibitory ensembles tend to stabilize the in-phase synchronization. Moreover, it was found that the inter-module synchronization is more noticeable when the inner-module synchronization is weak. The final section provides a discussion and conclusions.

2 One-Module System

In this section, we consider a module of a pulse neural network composed of excitatory neurons with internal states $\theta_E^{(i)}$ ($i = 1, 2, \cdots, N_E$) and inhibitory neurons with internal states $\theta_I^{(i)}$ ($i = 1, 2, \cdots, N_I$) that are written as

$$\dot{\theta}_E^{(i)} = (1 - \cos\theta_E^{(i)}) + (1 + \cos\theta_E^{(i)})$$
$$\times (r_E + \xi_E^{(i)}(t) + g_{EE}I_E(t) - g_{EI}I_I(t)) \quad (2.1)$$

$$\dot{\theta}_I^{(i)} = (1 - \cos\theta_I^{(i)}) + (1 + \cos\theta_I^{(i)})$$
$$\times (r_I + \xi_I^{(i)}(t) + g_{IE}I_E(t) - g_{II}I_I(t)), \quad (2.2)$$

$$I_X(t) = \frac{1}{N_X} \sum_{i=1}^{N_X} \delta(\theta_X^{(i)} - \pi), \quad (2.3)$$

$$\langle \xi_X^{(i)}(t)\xi_Y^{(j)}(t') \rangle = D\delta_{XY}\delta_{ij}\delta(t - t'), \quad (2.4)$$

where $X, Y = E$ or I, g_{XY} is the connection strength from ensemble Y to ensemble X, r_E and r_I are system parameters, and δ_{XY} and δ_{ij} are Kronecker's deltas. $I_X(t)$ is the synaptic inputs from ensemble X, and $\xi_X^{(i)}(t)$ is noise in the i-th neuron in ensemble X. In the following, we call this network with excitatory and inhibitory ensembles as the one-module system. The dynamics of this one-module system are nearly identical with the dynamics of the pulse-coupled active rotators analyzed by

Kanamaru and Sekine (2005). Therefore, we will briefly describe it here. Note that the model of neurons with $\dot{\theta} = (1 - \cos\theta) + (1 + \cos\theta)r$ is the canonical model of class 1 neurons (Ermentrout & Kopell, 1986; Ermentrout, 1996), and arbitrary class 1 neurons near their bifurcation points can be transformed into the canonical model. The canonical model was previously extended to the network of weakly connected class 1 neurons (Hoppensteadt & Izhikevich, 1997; Izhikevich, 1999), and the system governed by equations 2.1, 2.2, and 2.3 has the form of this canonical model of weakly connected class 1 neurons. Thus, the networks of the weakly connected arbitrary class 1 neurons with global connections can be transformed into the above form with the appropriate change of variables. Here we restrict the parameters so that the system parameters r_E and r_I and the noise intensity D are uniform in the network. Moreover, the restrictions $g_{EE} = g_{II} \equiv g_{int} = 4$ and $g_{EI} = g_{IE} \equiv g_{ext}$ are placed on the connection strengths for simplicity.
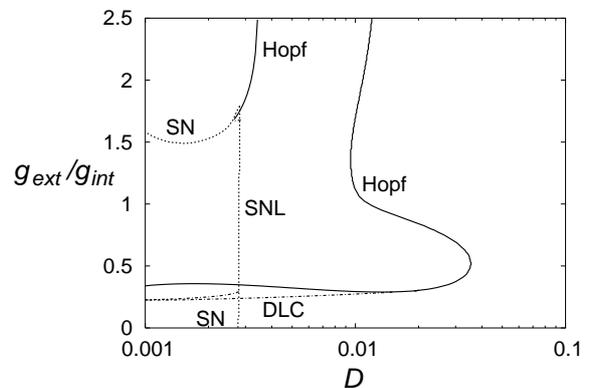
Figure 1: Bifurcation set in the (D, g_{ext}) plane for $r_E = -0.025$ and $r_I = -0.05$. SN, saddle-node; SNL, saddle-node-on-limit-cycle; DLC, double limit cycle.

In the absence of noise $\xi_X^{(i)}(t)$ and synaptic input $I_X(t)$, a single neuron shows self-oscillation for $r_X > 0$. For $r_X < 0$, this neuron becomes an excitable system with a stable equilibrium written by

$$\theta_0 = -\arccos\frac{1 + r_X}{1 - r_X}, \quad (2.5)$$

in which θ_0 is close to zero for $r_X \sim 0$. We define the firing time of the neuron as the time at which $\theta_X^{(i)}$ exceeds π because π is away from θ_0 (~ 0). Note that the relation $\dot{\theta}_E^{(i)} = \dot{\theta}_I^{(i)} = 2 > 0$ holds at $\theta = \pi$ independent of the synaptic input $I_X(t)$ and the noise $\xi_X^{(i)}(t)$; therefore the firing of the neuron can be defined naturally. In the following, we use values of the parameter where $r_X < 0$ and we consider the dynamics of the networks of excitable neurons.

Note that the synaptic input $I_X(t)$ from ensemble X

2
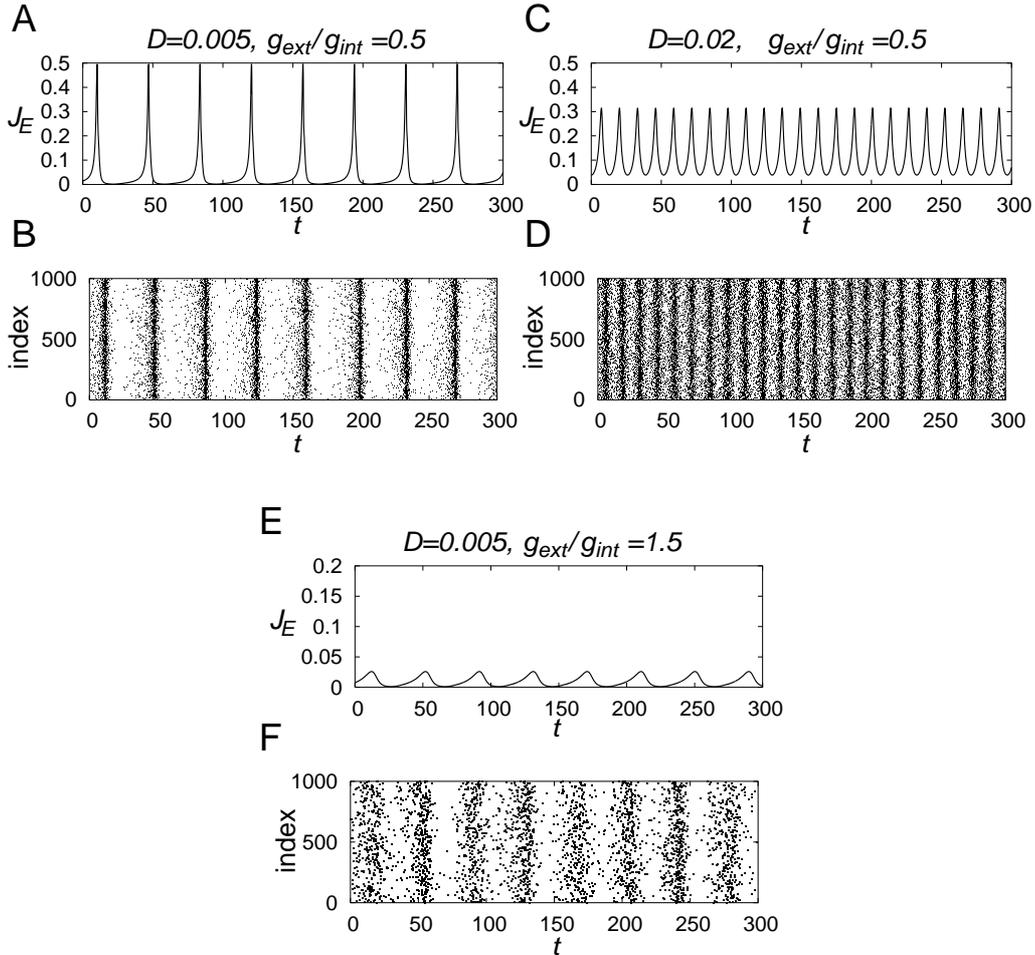
Figure 2: Synchronized firings of neurons in the one-module system in the case where $r_E = -0.025$ and $r_I = -0.05$. (A), (C), and (E) Change in the probability flux J_E over time at $\theta_E = \pi$. (B), (D), and (F) Raster plots of the firing times of the excitatory neurons in the system with $N_E = N_I = 1000$. (A), (B) Synchronized firings of neurons where D and g_{ext}/g_{int} are near the saddle-node-on-limit-cycle bifurcation. The results in the case of $D = 0.005$, $g_{ext}/g_{int} = 0.5$, and $g_{int} = 4$ are shown. (C), (D) Synchronized firings of neurons where D and g_{ext}/g_{int} are near the Hopf bifurcation. The results in the case of $D = 0.02$, $g_{ext}/g_{int} = 0.5$, and $g_{int} = 4$ are shown. (E), (F) Weakly synchronized periodic firings of neurons where $D = 0.005$, $g_{ext}/g_{int} = 1.5$, and $g_{int} = 4$.

can be rewritten as

$$I_X(t) = \frac{1}{2N_X} \sum_{i=1}^{N_X} \sum_j \delta(t - t_j^{(i)}), \qquad (2.6)$$

where $t_j^{(i)}$ is the j-th firing time of the i-th neuron in ensemble X.

In the limit of $N_E, N_I \to \infty$, the average behavior of neurons in the system can be analyzed with the Fokker-Planck equations which describe the development of the probability density of the system over time as shown in Appendix A. It is notable that asynchronous firings and synchronized firings of neurons in the network correspond to a stationary solution and a time-varying solution of the Fokker-Planck equations, respectively. Using the Fokker-Planck equations, a bifurcation set is obtained numerically by the method shown in Appendix B,

and the bifurcation set for the parameters $r_E = -0.025$ and $r_I = -0.05$ is shown in Figure 1. Generally, synchronized firings of neurons are observed when the chosen values of noise intensity D and connection strength g_{ext} are in the area enclosed by the SNL (saddle-node-on-limit-cycle) and Hopf bifurcation lines (Figure 1). For more detailed information about the bifurcation, please see the paper published by Kanamaru and Sekine (2005).

Typical synchronized firings of neurons in a one-module system are shown in Figure 2. The change in the probability flux J_E, which is defined in Appendix A, at $\theta_E = \pi$ over time for various values of D and g_{ext}/g_{int}, are shown in Figures 2A, 2C, and 2E. Note that the probability flux J_E can be interpreted as the instantaneous firing rate of the excitatory ensemble. The raster plots of the firing times of the excitatory neurons in the system with $N_E = N_I = 1000$ are shown in Figures 2B, 2D, and

3

2F. As shown in Figures 2A and 2B, in cases where D and g_{ext}/g_{int} are near the saddle-node-on-limit-cycle bifurcation, the synchronized firings of neurons have strong correlations and long periods because the system stays a long time in the area where the original saddle and node existed. As shown in Figures 2C and 2D, in cases where D and g_{ext}/g_{int} are near the Hopf bifurcation, the synchronized firings of neurons have weak correlations and high frequencies because a limit cycle that corresponds to these synchronized firings is created around the stable equilibrium with large probability fluxes. The synchronized firings of neurons shown in Figures 2E and 2F are weakly synchronized periodic firings (Kanamaru & Sekine, 2004) where only a small percentage of the neurons fire in each period. Such firings are realized when the peak value of the probability flux J_E is very small as shown in Figure 2E, and when each neuron receives subthreshold periodic inputs. We assume that these weakly synchronized periodic firings may be related to the physiologically observed synchronized firings because their degree of synchronization is also weak (Gray & Singer, 1989; Buzsáki, Horváth, Urioste, Hetke, & Wise, 1992; Fisahn, Pike, Buhl, & Paulsen, 1998). However, in the physiological environment, the properties of single neurons are not uniform and the structures of the networks are more complex. Therefore, more detailed theoretical analyses are required to validate the presence of neurons with weakly synchronized periodic firings in physiological environments.

3   Two-Module System

In this section, to study the mechanism of the synchronized oscillations among distant neurons, we consider the two-module system in which the internal states of the neurons are defined as:

$$\dot{\theta}_{E_k}^{(i)} = (1 - \cos\theta_{E_k}^{(i)}) + (1 + \cos\theta_{E_k}^{(i)})$$
$$\times (r_{E_k} + \xi_{E_k}^{(i)}(t) + g_{E_k E_k} I_{E_k}(t) - g_{E_k I_k} I_{I_k}(t)$$
$$+ \epsilon_{E_k E_l} I_{E_l}(t) - \epsilon_{E_k I_l} I_{I_l}(t)), \qquad (3.1)$$

$$\dot{\theta}_{I_k}^{(i)} = (1 - \cos\theta_{I_k}^{(i)}) + (1 + \cos\theta_{I_k}^{(i)})$$
$$\times (r_{I_k} + \xi_{I_k}^{(i)}(t) + g_{I_k E_k} I_{E_k}(t) - g_{I_k I_k} I_{I_k}(t),$$
$$+ \epsilon_{I_k E_l} I_{E_l}(t) - \epsilon_{I_k I_l} I_{I_l}(t)), \qquad (3.2)$$

$$l \equiv 3 - k, \qquad (3.3)$$

where $k = 1, 2$ and represents the first and second modules, respectively. For simplicity, we set the inner-module connection strengths as $g_{X_k Y_k} = g_{XY}$ and the inter-module connection strengths as $\epsilon_{X_k Y_l} \equiv \epsilon_{XY} (k \neq l)$. Moreover, we assume that the inter-module connection strengths are very weak, namely, $\epsilon_{XY} \ll 1$, and that the inter-module connections originate only from the excitatory ensembles, namely, $\epsilon_{EI} = \epsilon_{II} = 0$, because the inter-columnar long-range connections in the cortex are excitatory (Gilbert & Wiesel, 1983; Ts'o, Gilbert, & Wiesel, 1986).
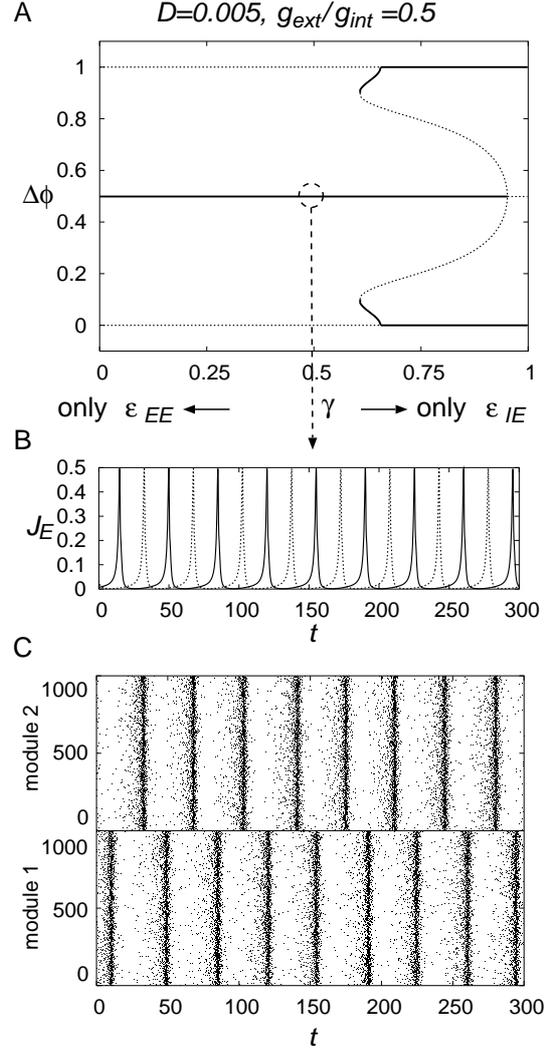
Figure 3: (A) Dependence of the stationary phase differences between the two modules of a two-module system on the connection ratio γ in the case where $r_E = -0.025$, $r_I = -0.05$, $D = 0.005$, $g_{ext}/g_{int} = 0.5$, and $g_{int} = 4$. The phase variable is normalized with the period T. The solid and dotted lines denote the stable and unstable phase differences, respectively. (B) Change in J_E over time in the case where $\gamma = 0.5$. The solid and dotted lines denote modules 1 and 2, respectively. (C) Raster plot of the firing times of excitatory neurons in a two-module system where $N_E = N_I = 1000$. In (B) and (C), the inter-module connection strengths were set at $\epsilon_{EE} = \epsilon_{IE} = 0.025$.

A similar network of two modules, each of which contains an excitatory cell (E-cell) and an inhibitory cell (I-cell), was previously analyzed by Ermentrout and Kopell (1998). The E-cell and I-cell each represented populations of neurons, and their dynamics obeyed the equations for the spiking neuron model. The neurons in each population were assumed to have perfectly synchronized firings. However, as shown in Figure 2, our inner-

module neurons do not show perfectly synchronized firings; therefore, the average behavior of the neurons in each module cannot be represented by that of a single neuron. Instead, we use the probabilistic representation of the Fokker-Planck equation to describe the dynamics of each module.

A $D=0.02$, $g_{ext}/g_{int}=0.5$

only ϵ_{EE} ⟵ γ ⟶ only ϵ_{IE}

B

C
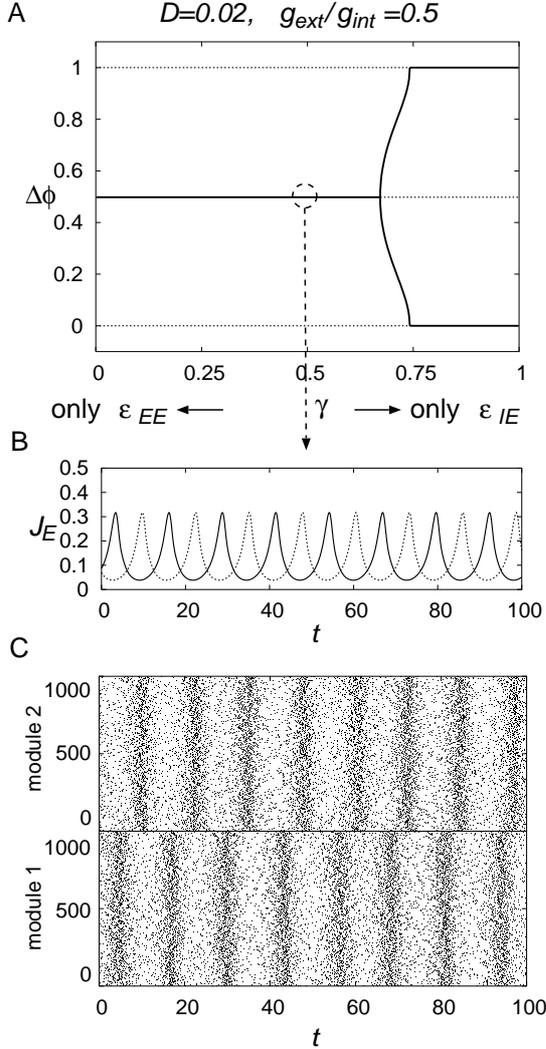
Figure 4: Dependence of the stationary phase differences between the two modules of a two-module system on the connection ratio γ in the case where $D = 0.02$, $g_{ext}/g_{int} = 0.5$, and $g_{int} = 4$. The explanations are the same as those in Figure 3 except for the values of the parameters.

In the limit of $N_{E_k}, N_{I_k} \to \infty$, the dynamics of the probability density of each module are governed by the Fokker-Planck equation shown in Appendix A, and the Fourier coefficients of the probability densities follow the ordinary differential equation $\dot{\boldsymbol{x}} = \boldsymbol{f}(\boldsymbol{x})$, which is defined in Appendix B. When each module shows inner-module synchronized firings, the vector $\boldsymbol{x}$ moves on a limit cycle $\boldsymbol{x} = \boldsymbol{x}_0(t)$. In a system of two modules that have weak inter-module connections ϵ_{XY}, the two limit

cycles are connected weakly, and such system can be analyzed using the phase response function (Kuramoto, 1984; Ermentrout & Kopell, 1991; Ermentrout, 1996; Ermentrout, Pascal, & Gutkin, 2001; Nomura, Fukai, & Aoyagi, 2003), as summarized in Appendix C. Using this method, we can transform the weakly connected ordinary differential equation $\dot{\boldsymbol{x}} = \boldsymbol{f}(\boldsymbol{x})$ of the Fourier coefficients into the averaged phase equations C.5 and C.6, and we can analyze the stationary phase differences using C.10.

A $D=0.005$, $g_{ext}/g_{int}=1.5$

only ϵ_{EE} ⟵ γ ⟶ only ϵ_{IE}

B

C
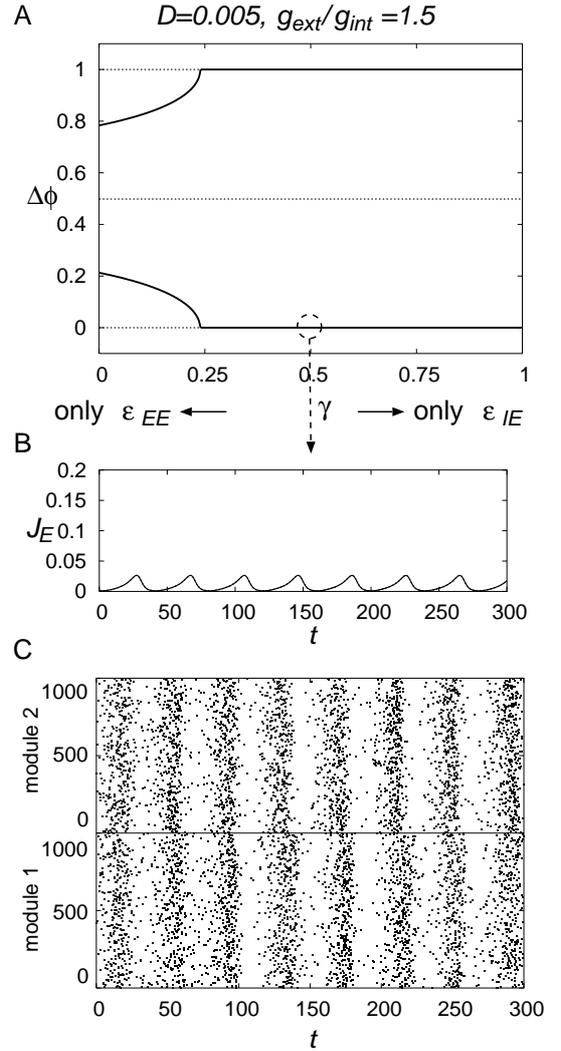
Figure 5: Dependence of the stationary phase differences between the two modules of a two-module system on the connection ratio γ in the case where $D = 0.005$, $g_{ext}/g_{int} = 1.5$, and $g_{int} = 4$. The explanations are the same as those in Figure 3 except for the values of the parameters.

The dependence of the stationary phase differences on the ratio γ, which is defined as

$$\epsilon_{EE} : \epsilon_{IE} = 1 - \gamma : \gamma, \qquad (3.4)$$

in cases with different values of D and g_{ext}/g_{int} is shown
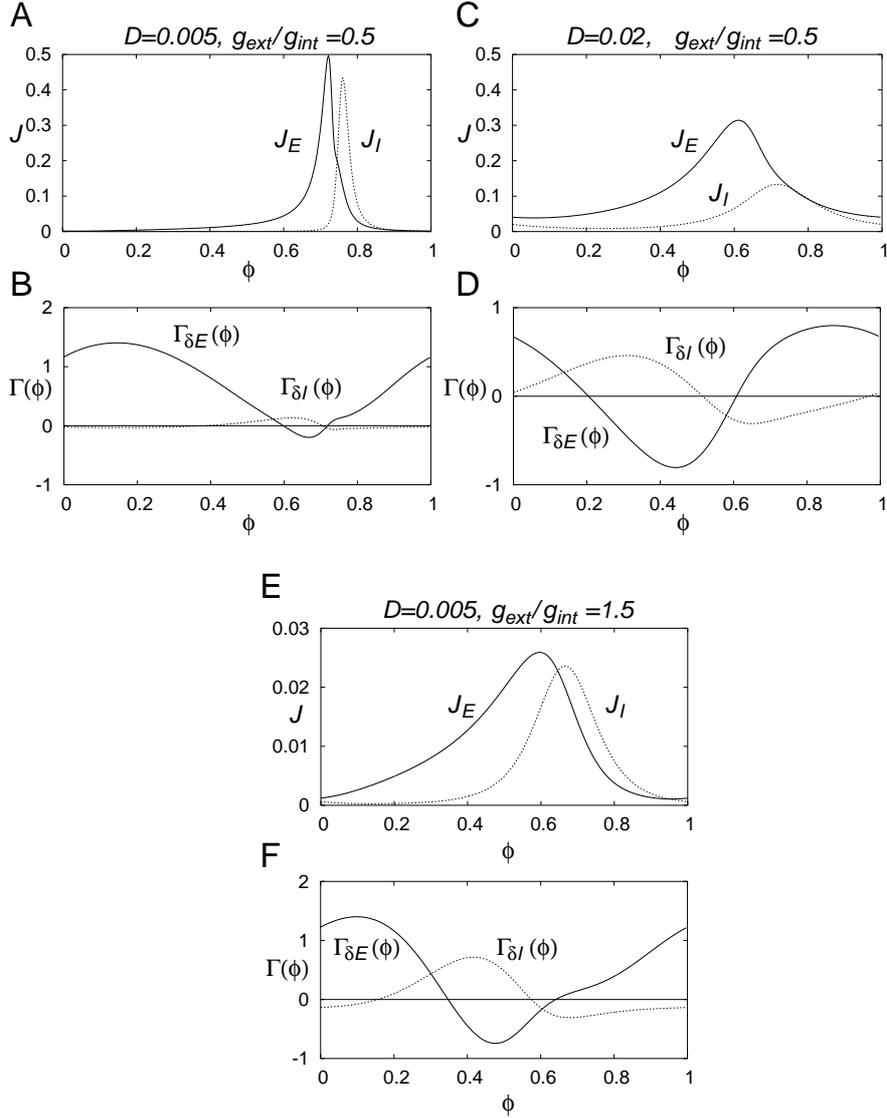
Figure 6: The phase responses $\Gamma_{\delta E}$ and $\Gamma_{\delta I}$ upon injection of the delta function to the excitatory or inhibitory ensemble, respectively. (A), (C), and (E) Change in J_E and J_I over time during a single period. (B), (D), and (F) Phase responses. The parameters are shown in each figure.

in Figures 3, 4, and 5. In the following, in-phase and anti-phase synchronizations are defined as the stationary solution with phase difference $\Delta\phi = 0$ or $\Delta\phi = 0.5$, respectively. In all cases, it was found that the connections from excitatory to excitatory ensembles (ϵ_{EE}) tended to stabilize the anti-phase synchronization, while the connections from excitatory to inhibitory ensembles (ϵ_{IE}) tended to stabilize the in-phase synchronization. However, when the inner-module synchronizations were strong (Figure 3), the anti-phase synchronization remained stable even when ϵ_{IE} was large, and therefore inter-module synchronization was harder to attain than in other cases. On the other hand, when the inner-module synchronizations were weak (Figure 5), the in-phase synchronization was stable over a wide range of γ, and therefore inter-module synchronization was eas-

ily attained.

As shown above, ϵ_{EE} and ϵ_{IE} contribute to the inter-module synchronization in different ways, because their phase responses have different properties. Note that the phase response describes the change in frequency at ϕ in response to small perturbations, as shown in Appendix C. The phase response function $\boldsymbol{Z}(t)$ is a vector function whose components represent the effects of inputs to the Fourier components of the Fokker-Planck equation. To make the phase response easier to understand, the phase responses $\Gamma_{\delta E}$ and $\Gamma_{\delta I}$ upon injection of the delta function into the excitatory or inhibitory ensemble, are calculated by equation C.7 and the results are shown in Figure 6 for three sets of parameters. Generally, the two phase responses have opposite signs in three cases; therefore, it can be concluded that the connections to

excitatory and inhibitory ensembles have opposite synchronization properties. Moreover, when the system is close to the saddle-node-on-limit-cycle bifurcation point (Figures 3, 6A, and 6B), the phase response of the inhibitory ensemble is much smaller than that of the excitatory ensemble. Thus, the in-phase synchronization is hard to attain in Figure 3. Although the phase responses in Figures 6D and 6F have similar forms, the amplitude of J_I is smaller than that of J_E in Figure 6C. Thus, the effect of the inhibitory ensemble is weak when the system is close to the Hopf bifurcation point and its firing rates are high (Figures 4, 6C, and 6D), and the in-phase synchronization is harder to attain than the weakly synchronized periodic firings in Figure 5.

Next, let us consider a system with a transmission delay d between two modules. Such a system can be analyzed with the equation

$$\Gamma_d(\phi_\alpha - \phi_{\alpha'}) = \frac{1}{T} \int_0^T \boldsymbol{Z}(t + \phi_\alpha) \cdot \boldsymbol{p}(t + \phi_\alpha, t + \phi_{\alpha'} - d) dt,$$
(3.5)

which was obtained by incorporating the delay d to $\Gamma(\phi_\alpha - \phi_{\alpha'})$ in equation C.7 (Hansel, Mato, & Meunier, 1995). The areas where the in-phase or anti-phase synchronization is stable are obtained numerically, and their dependence on the connection rate γ and the delay d is shown in Figure 7, where the delay is normalized by the period T. It is observed that in cases where d is small, ϵ_{IE} stabilizes the in-phase synchronization, and in cases where d is large, ϵ_{EE} stabilizes the in-phase synchronization. Let us consider the physiologically valid values of d for a gamma oscillation of 40 Hz ($T = 25$ ms). The major components of the delay in signal transmission between two neurons are transmission delay on the axon and the synaptic delay to transmit the signal across the synaptic cleft (Nicholls, Martin, Wallace, & Fuchs, 2001). Because the conduction velocity along a myelinated axon is $1 \sim 100$ m/s, the conduction delay between two neurons separated by 7 mm is estimated to be $0.07 \sim 7$ ms. The synaptic delay is known to be about $1 \sim 2$ ms. Thus, we roughly estimated that $d < 10$ ms and obtained the relationship $d/T < 0.4$. Under this condition, ϵ_{IE} stabilizes the in-phase synchronization, as shown in Figure 7. Moreover, for $d/T < 0.4$, the area with stable in-phase synchronization was widest for the weakly synchronized periodic firings (Figure 7C).

4 Discussion and Conclusions

To study the mechanism through which synchronized oscillations occur in the brain, we analyzed the properties of synchronization of class 1 pulse neural networks.

In the one-module system which was composed of excitatory and inhibitory neurons, various synchronized firings were observed depending on the connection strengths and the noise intensity, and they might be related to the synchronized oscillations with gamma frequency among nearby neurons in the visual cortex.

Note that such synchronized firings can be observed only when the excitatory neurons and inhibitory neurons are connected with each other (see the area with $g_{ext} = 0$ in Figure 1). In other words, the synchronized firings observed in our model were generated by the interactions between the excitatory ensemble and inhibitory ensemble in the network. On the other hand, it is known that self-oscillating neurons that consist of only excitatory (or inhibitory) neurons in a network can synchronize with each other (Mirollo & Strogatz, 1990). This difference might arise because our network is composed of excitable, but not self-oscillating, neurons.

To elucidate the mechanism by which synchronized oscillations occur among distant neurons, we analyzed the synchronization between two modules of networks using the phase response function. A similar network of two modules, each of which showed perfect synchronization, was previously analyzed by Ermentrout and Kopell (1998). However, as shown in Figure 2, the neurons in our module do not show perfect synchronization; therefore, a probabilistic representation with the Fokker-Planck equation was required to describe the dynamics of each module. As a result, it was found that the inter-module connections from excitatory to excitatory ($E \to E$) ensembles tended to stabilize the anti-phase synchronization, while the inter-module connections from excitatory to inhibitory ($E \to I$) ensembles tended to stabilize the in-phase synchronization. Moreover, it was found that inter-module synchronization was more easily attained when the inner-module synchronizations were weak.

Our finding that the $E \to E$ inter-module connections stabilize anti-phase synchronization is analogous to the previous results that a pair of excitatory neurons with slow connections have a stable anti-phase solution (Hansel, Mato, & Meunier, 1995; van Vreeswijk, 1996; Sato & Shiino, 2002). Moreover, our finding that the $E \to I$ inter-module connections tend to stabilize the in-phase synchronization, is similar to the previous result that the $E \to I$ and $I \to E$ connections stabilize the in-phase synchronization despite the existence of a delay (Ermentrout & Kopell, 1998). However, the mechanism of synchronization in their model differs from that in our model. In the model of Ermentrout and Kopell (1998), the timing of the pulses played important roles in synchronization because their network contained only four neurons, namely, two E-cells and two I-cells. They stated that a pair of pulses (doublet) of the I-cell was important in the process of synchronization. However, in our network, there are many neurons and each neuron receives many pulses from other neurons (see Figures 2B, 2D, and 2F). Therefore, the timing of the pulses is less important in our model than in their model. Nevertheless, similar results on the roles of $E \to I$ connections were obtained. Moreover, in our model, it was found that the degree of synchronization in one module affects the properties of the inter-module synchronization.

In summary, in our model, the oscillations in a neu-
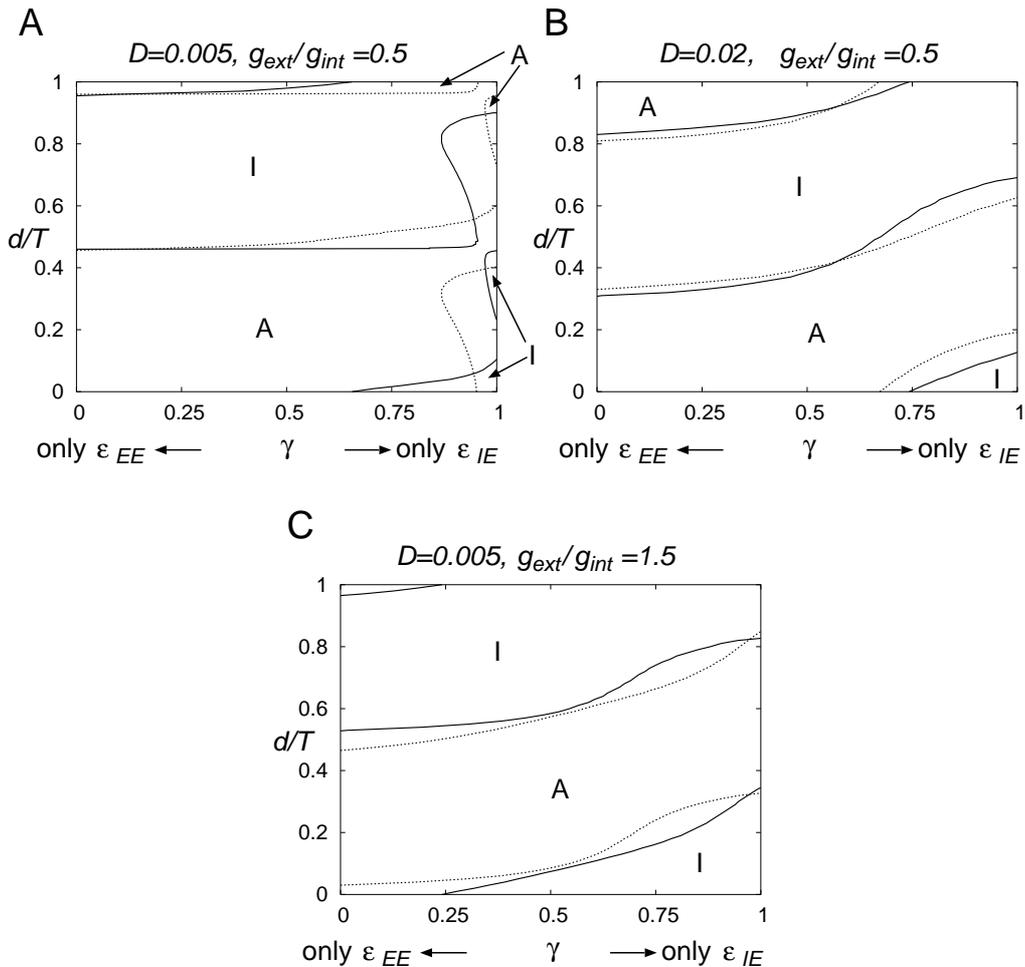
Figure 7: Areas where the in-phase or anti-phase synchronization is stable in the (γ, d) plane. The solid and dotted lines are the boundaries for the stable region of the in-phase or anti-phase synchronization, respectively. The delay d is normalized with the period T. The in-phase synchronization is stable in the areas labeled "I", and, the anti-phase synchronization is stable in the areas labeled "A". The other stable phase differences are omitted for simplicity.

ronal ensemble were generated by a local network composed of excitatory neurons and inhibitory neurons, and their synchronization was realized by the long-range connections from excitatory to inhibitory ensembles. We modeled the average dynamics of the module using probabilistic representation with the Fokker-Planck equation. In physiological environments, the properties of single neurons are not uniform and the networks are more complex; therefore, probabilistic representation may be crucial for understanding their dynamics. However, in the present research, we assumed that the properties of the neurons and the structure of the module were uniform. Therefore, more detailed analyses are required. Moreover, we confirmed that the analysis with the phase response function is applicable to the stochastic system whose average dynamics obey the Fokker-Planck equation. It is known that the phase response function can be calculated from physiological data (Reyes & Fetz,

1993a,b; Jones, Mulloney, Kaper, & Kopell, 2003); therefore, our method might widen application of the phase response function in theoretical and experimental fields.

A   The Fokker-Planck Equation for the One-Module System

To analyze the dynamics of the one-module system, we use the Fokker-Planck equations (Kuramoto, 1984; Gerstner & Kistler, 2002) which are written as

$$
\begin{aligned}
\frac{\partial n_E}{\partial t} &= -\frac{\partial}{\partial \theta_E}(A_E n_E) \\
&\quad + \frac{D}{2}\frac{\partial}{\partial \theta_E}\left\{ B_E \frac{\partial}{\partial \theta_E}(B_E n_E) \right\}, \text{(A.1)} \\
\frac{\partial n_I}{\partial t} &= -\frac{\partial}{\partial \theta_I}(A_I n_I)
\end{aligned}
$$

$$+\frac{D}{2}\frac{\partial}{\partial\theta_I}\left\{B_I\frac{\partial}{\partial\theta_I}(B_I n_I)\right\}, \quad \text{(A.2)}$$

$$
\begin{aligned}
A_E(\theta_E,t) &= (1-\cos\theta_E)+(1+\cos\theta_E)\\
&\quad\times(r_E+g_{EE}I_E(t)-g_{EI}I_I(t)),\text{(A.3)}\\
A_I(\theta_I,t) &= (1-\cos\theta_I)+(1+\cos\theta_I)\\
&\quad\times(r_I+g_{EE}I_E(t)-g_{II}I_I(t)), \text{(A.4)}\\
B_E(\theta_E,t) &= 1+\cos\theta_E, \quad\quad\quad\quad\text{(A.5)}\\
B_I(\theta_I,t) &= 1+\cos\theta_I, \quad\quad\quad\quad\text{(A.6)}
\end{aligned}
$$

for the normalized number densities of excitatory and inhibitory neurons, in which

$$n_E(\theta_E,t) \equiv \frac{1}{N_E}\sum_{i=1}^{N_E}\delta(\theta_E^{(i)}-\theta_E), \quad\text{(A.7)}$$

$$n_I(\theta_I,t) \equiv \frac{1}{N_I}\sum_{i=1}^{N_I}\delta(\theta_I^{(i)}-\theta_I), \quad\text{(A.8)}$$

in the limit of $N_E, N_I \to \infty$. The probability flux for each ensemble is defined as

$$J_E(\theta_E,t) = A_E n_E - \frac{D}{2}B_E\frac{\partial}{\partial\theta_E}(B_E n_E), \text{ (A.9)}$$

$$J_I(\theta_I,t) = A_I n_I - \frac{D}{2}B_I\frac{\partial}{\partial\theta_I}(B_I n_I), \quad\text{(A.10)}$$

respectively. In the limit of $N_X \to \infty$, $I_X(t)$ in equation 2.6 follows an equation that is written as

$$
\begin{aligned}
I_X(t) &= \frac{1}{2}J_X(t), \quad\quad\quad\quad\text{(A.11)}\\
&= n(\pi,t), \quad\quad\quad\quad\text{(A.12)}
\end{aligned}
$$

where $J_X(t) \equiv J_X(\pi,t)$ is the probability flux at $\theta_X = \pi$.

By integrating the Fokker-Planck equations A.1 and A.2 with equation A.12, the dynamics of the network governed by equations 2.1 and 2.2 can be analyzed.

B Numerical Integration of the Fokker-Planck Equations

In this section, we provide a method of performing numerical integration of the Fokker-Planck equations A.1 and A.2. Because the normalized number densities given by equations A.7 and A.8 are 2π-periodic functions of θ_E and θ_I, respectively, they can be expanded as

$$n_E(\theta_E,t) = \frac{1}{2\pi}+\sum_{k=1}^{\infty}(a_k^E(t)\cos(k\theta_E)+b_k^E(t)\sin(k\theta_E)),$$
$$\text{(B.1)}$$

$$n_I(\theta_I,t) = \frac{1}{2\pi}+\sum_{k=1}^{\infty}(a_k^I(t)\cos(k\theta_I)+b_k^I(t)\sin(k\theta_I)),$$
$$\text{(B.2)}$$

and, by substituting them, equations A.1 and A.2 are transformed into an ordinary differential equation $\dot{\boldsymbol{x}} =$ $\boldsymbol{f}(\boldsymbol{x})$ where $\boldsymbol{x} \equiv (a_1^E, b_1^E, a_1^I, b_1^I, a_2^E, b_2^E, a_2^I, b_2^I, \cdots)^t$,

$$
\begin{aligned}
\frac{da_k^{(X)}}{dt} &= -(r_X+K_X+1)kb_k^{(X)}\\
&\quad -(r_X+K_X-1)\frac{k}{2}(b_{k-1}^{(X)}+b_{k+1}^{(X)})\\
&\quad -\frac{Dk}{8}g(a_k^{(X)}), \quad\quad\quad\quad\text{(B.3)}\\
\frac{db_k^{(X)}}{dt} &= (r_X+K_X+1)ka_k^{(X)}\\
&\quad +(r_X+K_X-1)\frac{k}{2}(a_{k-1}^{(X)}+a_{k+1}^{(X)})\\
&\quad -\frac{Dk}{8}g(b_k^{(X)}), \quad\quad\quad\quad\text{(B.4)}\\
g(x_k) &= (k-1)x_{k-2}+2(2k-1)x_{k-1}+6kx_k\\
&\quad +2(2k+1)x_{k+1}+(k+1)x_{k+2}, \quad\text{(B.5)}\\
K_X &\equiv g_{XE}I_E-g_{XI}I_I, \quad\quad\quad\quad\text{(B.6)}\\
a_0^{(X)} &\equiv \frac{1}{\pi}, \quad\quad\quad\quad\quad\quad\quad\text{(B.7)}\\
b_0^{(X)} &\equiv 0, \quad\quad\quad\quad\quad\quad\quad\text{(B.8)}
\end{aligned}
$$

and $X = E$ or I. By integrating this ordinary differential equation numerically, the time series of the probability fluxes J_E and J_I are obtained. For numerical calculations, each Fourier series is truncated at the first 40 or 60 terms.

The bifurcation lines of the Hopf bifurcation and the saddle-node bifurcation in Figure 1 were obtained as follows. First, a stationary solution $\boldsymbol{x}_s$ was numerically obtained by the Newton method (Press, Flannery, Teukolsky, & Vetterling, 1988), and the eigenvalues of the Jacobian matrix $D\boldsymbol{f}(\boldsymbol{x}_s)$ which had been numerically obtained by using the QR algorithm (Press, Flannery, Teukolsky, & Vetterling, 1988), were examined to find the bifurcation lines. On the other hand, the bifurcation lines of the global bifurcations such as the homoclinic bifurcation and the double limit-cycle bifurcation, were obtained by observing the long-time behaviors of the solutions of $\dot{\boldsymbol{x}} = \boldsymbol{f}(\boldsymbol{x})$.

C Analysis with the Phase Response Function

In this section, we summarize the method of analyzing the dynamics of two weakly coupled oscillators.

Let us consider a dynamical system $\dot{\boldsymbol{x}} = \boldsymbol{f}(\boldsymbol{x})$ that has a stable limit cycle with period T as its solution, which was written as $\boldsymbol{x} = \boldsymbol{x}_0(t)$ ($\boldsymbol{x}_0(t) = \boldsymbol{x}_0(t+T)$), and then introduce a weak perturbation $\boldsymbol{p}(\boldsymbol{x},\boldsymbol{x}')$ from the other module $\boldsymbol{x}'$. Then, the dynamics of the module are governed by a differential equation written as

$$\dot{\boldsymbol{x}} = \boldsymbol{f}(\boldsymbol{x}) + \boldsymbol{p}(\boldsymbol{x},\boldsymbol{x}'), \quad\quad\text{(C.1)}$$

and it can be reduced to

$$\dot{\phi} = 1 + \boldsymbol{Z}(\phi)\cdot\boldsymbol{p}(\boldsymbol{x}_0,\boldsymbol{x}_0'), \quad\quad\text{(C.2)}$$

where $\phi = t \bmod T$ and $\boldsymbol{Z}(\phi)$ is the phase response function that describes the change in frequency at ϕ in response to small perturbations (Kuramoto, 1984; Ermentrout & Kopell, 1991 ;Ermentrout, 1996; Ermentrout, Pascal, & Gutkin, 2001; Nomura, Fukai, & Aoyagi, 2003). $\boldsymbol{Z}(\phi)$ can be numerically obtained using the method shown by Ermentrout (1996). First, let us consider a linear differential equation

$$\dot{\boldsymbol{Z}} = -D\boldsymbol{f}(\boldsymbol{x}_0(t))^t \cdot \boldsymbol{Z}(t), \qquad (C.3)$$

and integrate backward in time with random initial conditions. After $\boldsymbol{Z}(t)$ converges to a periodic orbit, normalization

$$\frac{1}{T}\int_0^T \boldsymbol{Z}(t) \cdot \dot{\boldsymbol{x}}_0(t)dt = 1 \qquad (C.4)$$

is performed, and $\boldsymbol{Z}(t)$ is obtained. Let us denote the phases of the two modules as ϕ_1 and ϕ_2, respectively. After averaging, the two phases obey

$$\dot{\phi}_1 = 1 + \Gamma(\phi_1 - \phi_2), \qquad (C.5)$$
$$\dot{\phi}_2 = 1 + \Gamma(\phi_2 - \phi_1), \qquad (C.6)$$
$$\Gamma(\phi_\alpha - \phi_{\alpha'}) = \frac{1}{T}\int_0^T \boldsymbol{Z}(t + \phi_\alpha) \cdot \boldsymbol{p}(t + \phi_\alpha, t + \phi_{\alpha'})dt, \qquad (C.7)$$
$$\boldsymbol{p}(t + \phi_\alpha, t + \phi_{\alpha'}) = \boldsymbol{p}(\boldsymbol{x}_0(t + \phi_\alpha), \boldsymbol{x}_0(t + \phi_{\alpha'})). \qquad (C.8)$$

Using $\Gamma(\phi)$, the phase difference $\Delta\phi \equiv \phi_1 - \phi_2$ of the two phases obeys

$$\dot{\Delta\phi} = \Gamma(\Delta\phi) - \Gamma(-\Delta\phi), \qquad (C.9)$$
$$\equiv \Gamma_{odd}(\Delta\phi). \qquad (C.10)$$

We can obtain the stable phase difference $\Delta\phi$ which satisfies $\Gamma_{odd}(\Delta\phi) = 0$ and $\Gamma'_{odd}(\Delta\phi) < 0$.

Acknowledgement

References
Bragin, A., Jandó, G., Nádasdy, Z., Hetke, J., Wise, K., & Buzsáki, G. (1995). Gamma (40-100Hz) oscillation in the hippocampus of the behaving rat. *J. Neurosci.*, 15, 47–60.

Buzsáki, G., Horváth, Z., Urioste, R., Hetke, J., & Wise, K. (1992). High-frequency network oscillation in the hippocampus. *Science*, 256, 1025–1027.

Cunningham, M. O., Davies, C. H., Buhl, E. H., Kopell, N., & Whittington, M. A. (2003). Gamma oscillations induced by kainate receptor activation in the entorhinal cortex in vitro. *J. Neurosci.*, 23, 9761–9769.

Ermentrout, B. (1996). Type I membranes, phase resetting curves, and synchrony. *Neural Comput.*, 8, 979–1001.

Ermentrout, G. B., & Kopell, N. (1986). Parabolic bursting in an excitable system coupled with a slow oscillation. *SIAM J. of Appl. Math.*, 46, 233–253.

Ermentrout, G. B., & Kopell, N. (1991). Multiple pulse interactions and averaging in systems of coupled neural oscillators. *J. Math. Biol.*, 29, 195–217.

Ermentrout, G. B., & Kopell, N. (1998). Fine structure of neural spiking and synchronization in the presence of conduction delays. *Proc. Natl. Acad. Sci. USA*, 95, 1259–1264.

Ermentrout, B., Pascal, M., & Gutkin, B. (2001). The effects of spike frequency adaptation and negative feedback on the synchronization of neural oscillators. *Neural Comput.*, 13, 1285–1310.

Fisahn, A., Pike, F. G., Buhl, E. H., & Paulsen, O. (1998). Cholinergic induction of network oscillations at 40 Hz in the hippocampus in vitro. *Nature*, 394, 186–189.

Gerstner, W., & Kistler, W. (2002). Spiking Neuron Models. Cambridge Univ. Press, Cambridge.

Gilbert, C. D., & Wiesel, T.N. (1983). Clustered intrinsic connections in cat visual cortex. *J. Neurosci.*, 3, 1116–1133.

Gray, C. M. (1994). Synchronous oscillations in neuronal systems: mechanisms and functions. *J. Comput. Neurosci.*, 1, 11–38.

Gray, C. M., & McCormick, D. A. (1996). Chattering cells: Superficial pyramidal neurons contributing to the generation of synchronous oscillations in the visual cortex. *Science*, 274, 109–113.

Gray, C. M., & Singer, W. (1989). Stimulus-specific neuronal oscillations in orientation columns of cat visual cortex. *Proc. Natl. Acad. Sci. USA*, 86, 1698–1702.

Hansel, D., Mato, G., & Meunier, C. (1995). Synchrony in excitatory neural networks. *Neural Comput.*, 7,

307–337.

Hoppensteadt, F. C., & Izhikevich, E.M. (1997). *Weakly Connected Neural Networks.* Springer, New York.

Izhikevich, E. M. (1999). Class 1 neural excitability, conventional synapses, weakly connected networks, and mathematical foundations of pulse-coupled models. *IEEE Trans. Neural Networks*, 10, 499–507.

Jagadeesh, B., Gray, C. M., & Ferster, D. (1992). Visually evoked oscillations of membrane potential in cells of cat visual cortex. *Science*, 257, 552–554.

Jones, S. R., Mulloney, B., Kaper, T. J., & Kopell, N. (2003). Coordination of cellular pattern-generating circuits that control limb movements: The sources of stable differences in intersegmental phases. *J. of Neurosci.*, 23, 3457–3468.

Kanamaru, T., & Sekine, M. (2004). An analysis of globally connected active rotators with excitatory and inhibitory connections having different time constants using the nonlinear Fokker-Planck equations. *IEEE Trans. Neural Networks*, 15, 1009–1017.

Kanamaru, T., & Sekine, M. (2005). Synchronized firings in the networks of class 1 excitable neurons with excitatory and inhibitory connections and their dependences on the forms of interactions. *Neural Comput.*, 17, 1315–1338.

Kuramoto, Y. (1984). *Chemical Oscillations, Waves, and Turbulence.* Springer, Berlin.

Mirollo, R. E., & Strogatz, S. H. (1990). Synchronization of pulse-coupled biological oscillators. *SIAM J. Appl. Math.*, 50, 1645–1662.

Nicholls, J. G., Martin, A. R., Wallace, B. G., & Fuchs, P. A. (2001). *From Neuron to Brain.* Sinauer Associates Inc. Publishers, Massachusetts.

Nomura, M., Fukai, T., & Aoyagi, T. (2003). Synchrony of fast-spiking interneurons interconnected by GABAergic and electrical synapses. *Neural Comput.*, 15, 2179-2198.

Press, W. H., Flannery, B. P., Teukolsky, S. A., & Vetterling, W. T. (1988). *Numerical Recipes in C.* Cambridge Univ. Press, New York.

Reyes, A. D., & Fetz, E. E. (1993a). Two modes of interspike interval shortening by brief transient depolarizations in cat neocortical neurons. *J. Neurophysiol.*, 69, 1661–1672.

Reyes, A. D., & Fetz, E. E. (1993b). Effects of transient depolarizing potentials on the firing rate of cat neocortical neurons. *J. Neurophysiol.*, 69, 1673–1683.

Sato, Y. D., & Shiino, M. (2002). Spiking neuron models with excitatory or inhibitory synaptic couplings and synchronization phenomena. *Phys. Rev. E*, 66, 041903.

Traub, R. D., Bibbig, A., LeBeau, F. E. N., Cunningham, M. O., & Whittington, M. A. (2005). Persistent gamma oscillations in superficial layers of rat auditory neocortex: experiment and model. *J. Physiolo.*, 562, 3–8.

Ts'o, D. Y., Gilbert, C. D., & Wiesel, T. N. (1986). Relationships between horizontal interactions and functional architecture in cat striate cortex as revealed by cross-correlation analysis. *J. Neurosci.*, 6, 1160–1170.

van Vreeswijk, C. (1996). Partial synchronization in populations of pulse-coupled oscillators. *Phys. Rev. E*, 54, 5522–5537.

Whittington, M. A., Traub, R. D., & Jefferys, J. G. R. (1995). Synchronized oscillations in interneuron networks driven by metabotropic glutamate receptor activation. *Nature*, 373, 612–615.